# Transonic Buffet Control on 3D Turbulent Wings using Fluidic Devices. Part 1: Open loop study

J. Dandois, J. Dor, P. Molton, A. Lepage, F. Ternoy, E. Coustols

# Transonic Buffet Control on 3D Turbulent Wings using Fluidic Devices. Part 1: Open loop study

**J. Dandois, J.-B. Dor, P. Molton, A. Lepage, F. Ternoy and E. Coustols**

*ONERA – The French Aerospace Lab*
*8 rue des Vertugadins 92190 MEUDON*

**Abstract:**

*This paper presents an overview of the work performed at Onera over the last decade on the control of the buffet phenomenon. This aerodynamic instability induces strong wall pressure fluctuations and as such limits aircraft envelope, consequently it is interesting to try to delay its onset, in order to improve aircraft performance, but also to provide more flexibility during the design phase. Several types of flow control have been investigated, either passive (mechanical vortex generators) or active (fluidic VGs, fluidic trailing-edge device (TED)). It is shown than mechanical and fluidic VGs are able to delay buffet onset in the angle-of-attack domain by suppressing the separation downstream of the shock. The effect of the fluidic TED is different, the separation is not suppressed but the rear wing loading is increased and consequently the buffet onset is not delayed to higher angles of attack, but only to higher lift coefficient. The objective of these wind tunnel tests was to prepare the closed-loop control of the buffet phenomenon, to adapt the mass flow rate to the aerodynamic conditions.*

**Résumé :**

*L'objectif de cet article est de présenter un résumé des activités réalisées à l'Onera ces dix dernières années sur le contrôle du tremblement. En effet, cette instabilité aérodynamique induit de fortes oscillations de pression à la paroi et par conséquent limite l'enveloppe de vol des avions. Il est donc intéressant d'essayer de retarder son apparition afin d'améliorer les performances aérodynamiques des avions d'une part et d'offrir plus de souplesse durant la phase de conception d'un nouvel avion d'autre part. Pour retarder l'apparition du tremblement, différents moyens de contrôle des écoulements ont été investigués soit passifs (générateur de tourbillons passifs ou VG) ou actifs (VG fluidiques, fente soufflant au bord de fuite à l'intrados (TED)). Il est démontré que les VGs passifs et fluidiques sont capables de repousser l'apparition du tremblement à des incidences plus élevées en supprimant le décollement en aval du choc. L'effet du TED fluidique est différent, le décollement n'est pas supprimé mais le chargement arrière de l'aile est augmenté et donc le tremblement n'est pas repoussé à des incidences plus élevées mais seulement à des coefficients de portance plus grand. L'objectif de ces essais en soufflerie était de préparer le contrôle en boucle fermée du tremblement dans le but d'adapter le débit aux conditions aérodynamiques afin de minimiser autant que possible celui-ci.*

**Key words:**

**Transonic ; Buffet ; Separation Control ; Vortex Generator ; Fluidic Control**.

## 1 Introduction

The shock-wave/boundary layer interaction on the upper side of a wing at high Mach number and/or high angle of attack induces a massive flow separation, which can lead to instability. This phenomenon is a global flow instability known as "buffet" and can further lead to structural vibrations ("buffeting"). Buffet results in lift and drag variations that greatly affect the aircraft aerodynamics and, as such, limit the aircraft flight envelope, since a margin of 30% on the lift coefficient at cruising conditions must be respected by design standards. For the last twenty-five

years or so, a structured multi-disciplinary research program has been defined at ONERA for addressing buffet characterization and control on, firstly turbulent airfoils, and then wings. This research program had comprised very detailed complementary experimental and numerical studies. Two complementary devices/technologies had been developed for buffet control:

- either a "VG-type" (Vortex Generator) actuator, the effect of which is to add momentum and kinetic energy to the turbulent boundary layer which develops upstream of the shock and the induced separation, in order to suppress, or at least to delay, the appearance of separated unsteady flows, which is at the origin of the buffet phenomenon;
- or a "TED-type" (Trailing Edge Device/Deflector) actuator, which behaves as a trailing edge, or cambered trailing edge, by increasing the rear loading of an aerofoil and then postponing the buffet onset at a higher lift coefficient.

At the beginning of 2007, a new joint ONERA research project was launched, aimed at controlling buffet studies on 3D turbulent wings [1]. The focus was to investigate buffet control via the use of fluidic devices, which should be easier to handle than mechanical TEDs for closed-loop control applications. In parallel to this research project, the EU-funded AVERT "Aerodynamic Validation of Emission Reducing Technologies" project, coordinated by Airbus Operations Ltd, was launched in January 2007. For high speed technologies, demonstration tests were focused on buffet control and were performed on a 3D half wing/fuselage body at the ONERA S2MA facility, in March 2010 [2]. Thus, the efficiency of delaying the buffet onset was shown using an open loop approach, with either fluidic VG or fluidic TED, at constant flow rate. The main characteristics of fluidic VGs and TED were defined by ONERA and LEA Poitiers [3], respectively.

In parallel, ONERA pursued buffet investigations on a 3D wing, the geometry of which being similar to that of the model tested at the ONERA S2MA wind tunnel, but adapted to fit in the test section of the "research-type" ONERA S3Ch wind tunnel [4].

Later on, within the framework of the Clean Sky SFWA-ITD "Smart Fixed Wing Aircraft – Integrated Technology Demonstrator", complementary high-speed tests were carried out on the 3D turbulent wing at the ONERA S3Ch wind tunnel in 2011, using fluidic VGs in open and closed loop.

This paper is aimed at providing the main outcomes from all these experimental tests.

## 2 Wind tunnel models

Before being performed in an "industrial-type" wind tunnel, tests have been carried out in the S3Ch wind tunnel of the ONERA Meudon Center. The objective of this test was to assess the efficiency of the fluidic VGs, by comparison with a more classical solution based on mechanical VGs. The experimental set-up is shown in Figure 1. The model is composed of a swept wing attached on a half-fuselage. This model was designed during the BUFET'N Co project and most of the wing is based on the supercritical OAT15A airfoil. The swept angle at the leading edge is equal to 30°. The wing twist was adapted to ensure a constant pressure along the span under cruising conditions, as well as a shock parallel to the leading edge. From root to tip, the chord varies between 240mm and 200mm over a span of 704mm. In the end, no separation at the wing root was ensured using adapted profiles and twist in that region.

Figure 1 - Experimental set-up in the S3Ch wind tunnel.

Then, after these first validation tests, wind tunnel test have been performed in the S2Ma wind tunnel of the ONERA Modane-Avrieux Center. This wind tunnel allows larger models to be tested. Moreover, it is equipped with a balance, which enables to study the buffet onset by varying the angle of attack of the model. Figure 2 shows the AVERT model in the S2Ma wind tunnel. The half-model geometry consists in a wing, a fuselage and a peniche. The wing cross-section geometry is based on the OAT15A airfoil, as for the S3Ch model in Figure 1. The wing span is larger (1.225 m) and the sweep angle is the same (30°). The chord length is 0.450 m at the wing root and 0.225 m at the wing tip. The mean aerodynamic chord is 0.3375 m.

Figure 2 – AVERT model in the S2MA wind tunnel.

## 3 Buffet control by passive VGs

As explained in Section 1, the first objective was to define a reference configuration with control, with which the others fluidic control devices like the fluidic VGs will be compared. It is well known that mechanical VGs are able to postpone buffet onset, so they have been chosen as a reference. Since the wing is swept, only co-rotating VGs are considered here. The VGs, whose vertices are located at 20% of the chord, consist in 27 small triangles with a height $h = \delta = 1.3$mm and a length equal to $5h$. Their skew angle has been defined using numerical simulations [5] and is equal to $\beta = 30°$ with respect to the freestream direction (and so $\beta = 0°$ with respect to the leading edge normal). The first VG is located at 51% of the span ($b$), the last one at 89%, and the spacing between the VGs is 1.7% of the span ($\lambda = 12h$). Figure 3 (bottom) shows an oil flow visualization of the controlled configurations with mechanical VGs. By comparing with the baseline without control (top), one can observe that flow separation has been suppressed over most of the wing span, except between $y/b = 0.5$ and 0.6 where a recirculation zone remains. Let us recall that VGs are only located at between 50% and 90% of the span, which leaves the first half of the wing uncontrolled and prone to separation, like for the baseline.

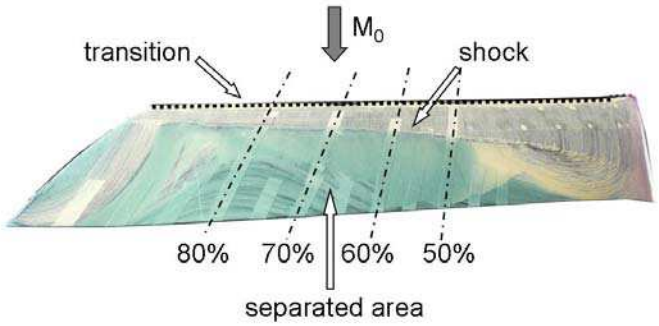

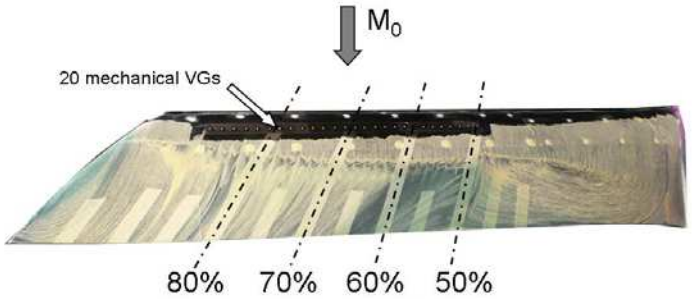

Figure 3 - Oil flow visualization without control (top) and with mechanical VGs (bottom) at $y/b$=75% (right) ($a$=3.5°, $M_0$=0.82).

## 4 Buffet control by fluidic VGs

### 4.1 Continuous blowing

On the S3Ch model, a cover with 40 co-rotating fluidic VGs has been manufactured to try to reproduce the effect of the mechanical VGs, with the advantage of being able to activate them only when they are necessary. The fluidic VGs consist in small nozzles with a conical shape and a supersonic exit flow at $M_{VG}$ = 2. The exit diameter of the nozzles ($d$) is equal to 1 mm and the pitch angle (defined between the jet direction and the local wall tangent, see Figure 4 (left)) is $\alpha$ = 30°. The 40 continuous fluidic VGs are located at between 53 and 82% of the span, with a spacing equal to 0.85% of the span ($\lambda$ = 6mm). A different cover with 25 pulsed fluidic VGs has also been manufactured. They are located at between 50 and 84% of the span with a spacing equal to 1.63% of the span ($\lambda$ = 11.5mm). The orientation of the jets with respect to the leading edge of the model $\beta$ being an important parameter, it has been studied numerically (Dandois et al. [5]), in order to define the most interesting skew angles to be tested. Thus, on the S3Ch model, two skew angles for continuous fluidic VGs have been tested: $\beta$ = 30° and 60° (and are named VGF4 and VGF5 respectively) and one for the pulsed fluidic VGs: $\beta$ = 60° (named VGFp). These pulsed fluidic VGs consist in ONERA home-made piezoelectric actuators supplied with compressed air and driven by an electric square signal. They are located at 23% of the chord.

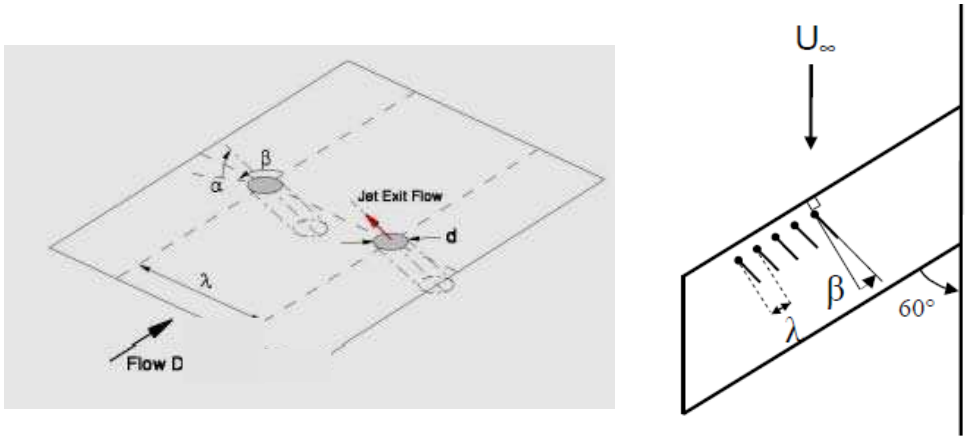

Figure 4 – Sketch showing the definitions of the main parameters of the fluidic VGs.

For the fluidic VGs, the momentum coefficient $C_\mu$ is defined by:

$$C_\mu = \frac{\rho_j S_j U_j^2}{\frac{1}{2}\rho_0 S U_0^2} = \frac{q_m U_j}{\frac{1}{2}\rho_0 S U_0^2}$$

where $\varrho_j$ and $U_j$ are respectively the density and velocity of the jets (time-averaged in the pulsed blowing case), $S_j$ the sum of all of the orifice surface area based on the hole diameter (not the projected surface) and $q_m$ is the mass flow rate (time-averaged in the pulsed blowing case). When the flow at the exit of the nozzles is supersonic, the Mach number ($M$ = 2) and thus $U_j$ are fixed and

only the mass flow rate continues to increase with the air supply stagnation pressure. The variables $\varrho_0$ and $U_0$ are, respectively, the freestream density and velocity of the main flow, the wing surface corresponding to a half span being denoted by $S$.

Figure 5 shows a comparison of the $Cp$ distributions at $y/b$ = 0.7 between the baseline, mechanical and fluidic VGs configurations. The results show that the control effect on the pressure plateau level upstream of the shock is negligible. The shock location has been shifted more downstream on the wing, at around $X/c$ = 0.55, because of the separation alleviation for all controlled cases. The shock seems to be located more downstream in the fluidic VGs case than for the mechanical VGs. For this value of the momentum coefficient $C_\mu$, which corresponds to a saturated effect of the fluidic VGs, the skew angle $\beta$ seems to have no effect on the wall pressure distribution.

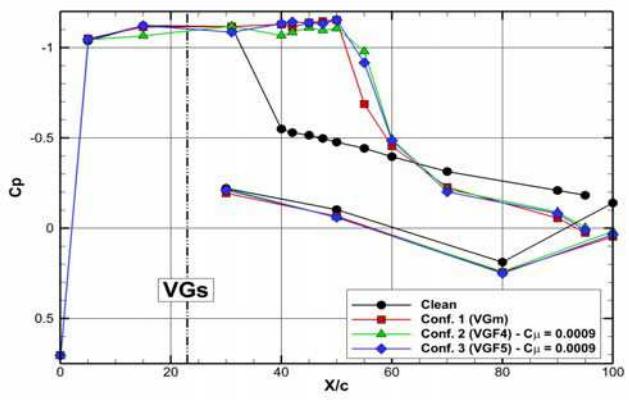


Figure 5 - Effect of the fluidic VGs mass flow rate on Cp distributions at $y/b$ = 0.7 ($\alpha$ = 3.5°, $M_0$ = 0.82).

The RMS pressure chordwise distributions at $y/b$ = 0.6 (only section equipped with Kulite sensors) of the clean and controlled configurations are compared in Figure 6. For the three controlled configurations, the maximum level corresponding to the crossing of the shock is located at about $x/c$ = 0.55. More downstream, the pressure fluctuation levels are lower in all controlled configurations than for the baseline. This confirms that unsteadiness in the separated region has been damped with either passive or active control. One can also note that the lowest levels are obtained by fluidic VGs. However, pressure fluctuation levels at the shock location are greater in the controlled cases than for the baseline, because the shock is located between two sensors for the baseline (see the shock position in Figure 6) and consequently the peak is not visible in the figure.

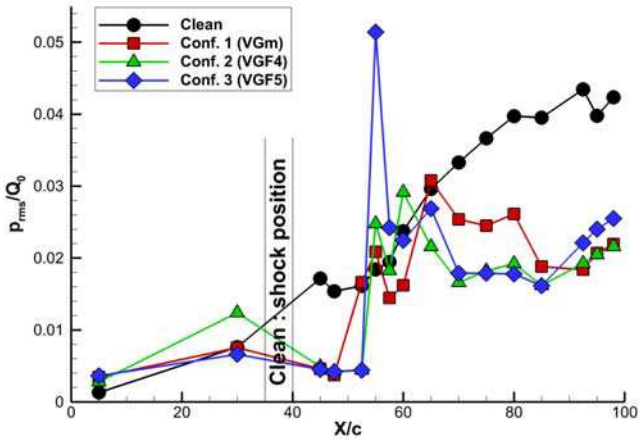


Figure 6 - Comparison of RMS pressure distributions at $Y/b$ = 0.6 ($\alpha$ = 3.5°, $M_0$ = 0.82).

This test case has been computed with the *elsA* software by Dandois *et al.* [5]. Figure 7 displays a Q-criterion iso-surface ($Q = 100U_\infty^2 / h^2$) coloured by the Mach number and the iso-surface $Vx = 0$ (streamwise velocity = 0, in black) for the fine overset grid. The streamwise vortices created by the co-rotating fluidic VGs are clearly visible. As observed in the experiment, there remains a small separated zone between 50 and 60% of the span.

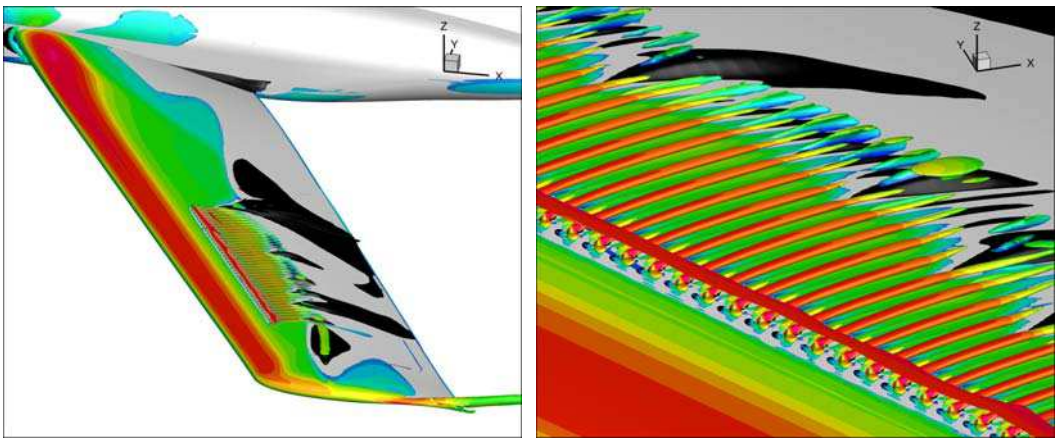

Figure 7 - Q-criterion iso-surface ($Q = 100U_\infty^2 / h^2$) coloured by the Mach number and separated zone (in black) showing the streamwise vortices created by the co-rotating fluidic VGs.

For the S2MA model, like for the S3Ch model, micro-nozzles with a throat diameter of 0.8 mm and an exit diameter $d = 1$ mm have been used. Since the model is larger than the S3Ch one, there are 50 fluidic VGs instead of 40. They are also located closer to the leading edge at 15% of the chord, in order to be outside the fuel tank region on a real aircraft. They are located between 46% and 89% of the wing span. The spacing between each hole is $\lambda = 14.4d$. Like for the S3Ch model, the pitch angle $a$ is fixed equal to 30°. Since on the S3Ch model no difference was observed between the two tested skew angles, only $\beta = 60°$ (taken from the normal to the leading edge line) has been tested on this model. The maximum mass flow is 0.5 g.s$^{-1}$ per hole and the fluidic VGs can operate in continuous blowing mode, or in pulsed blowing mode (between 0 and 700Hz) using piezoelectric actuators inside the model. Figure 8 shows a close-up view of the oil flow visualization of the controlled flow by fluidic VGs ($C_\mu = 5.8\ 10^{-4}$) at $a = 3°$. The streamwise vortices created by the VGs are traced by the streamwise line of oil washing between accumulations of blue oil. The shock foot is also modified by the interaction with the streamwise vortices. For a higher angle of attack $a = 4.25°$ (see Figure 9), in the uncontrolled case, the flow is separated on one third of the span in the central part, whereas in the controlled case with fluidic VGs, a flow separation starts to appear at around 40% of the span where the flow is not controlled (the fluidic VGs are located between 46 and 89% of the span). Thus, the fluidic VGs are able to delay the separation appearance as well as the mechanical VGs.

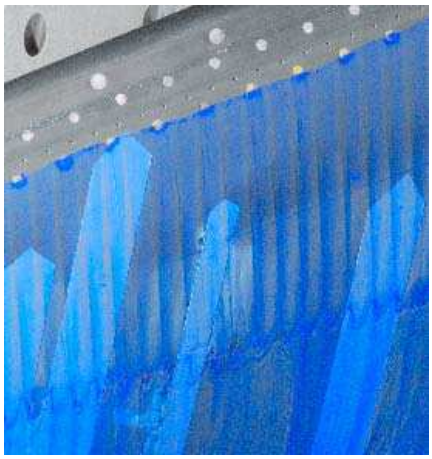

Figure 8 – Close-up view of the oil flow visualization around the fluidic VGs at $a$=3° and $C\mu$=5.8 $10^{-4}$ ($M$=0.82, $Re_c$=2.83 $10^6$).

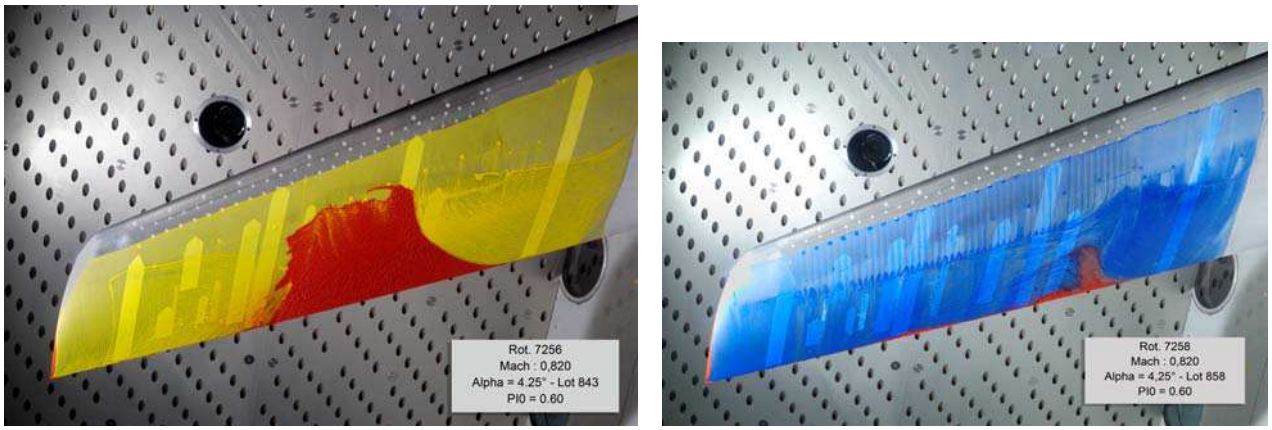


Figure 9 – Oil flow visualizations of the baseline (left) and the fluidic VGs case ($C\mu$=5.8 $10^{-4}$) at $a$=4.25°.

Since the S2MA wind tunnel is equipped with a balance, the effect of the fluidic VGs on lift and drag can be investigated. The lift change with the angle of attack is given in Figure 10 for the baseline, the mechanical VGs case and the fluidic VGs for some selected values of $C_\mu$. The control has no influence on the lift curves for $a$ < 2.5°. For $a$ > 2.5°, the lift curves of the baseline and the controlled case start to diverge, the control increases the lift. Then, for $a$ > 4°, the lift increment is nearly constant. The lift increment, observed for angles-of-attack larger than the buffet onset at $a$ = 3°, increases with $C_\mu$ but quickly reaches a saturation for $C_\mu \geq$ 4.6 $10^{-4}$ , which corresponds to a low value $C_\mu$ (5% of the maximum $C_\mu$) and the mass flow rate (5.9 $g.s^{-1}$ = ¼ of the maximum mass flow rate). The micro-nozzles are not even shocked. In Figure 10, the lift curves for $C_\mu$ = 4.6 $10^{-4}$ and 1.7 $10^{-3}$ are superimposed. The effect of the fluidic VGs on lift is comparable to the mechanical VGs one for a very low value of $C_\mu$ equal to 1.5 $10^{-4}$ (3 $g.s^{-1}$).

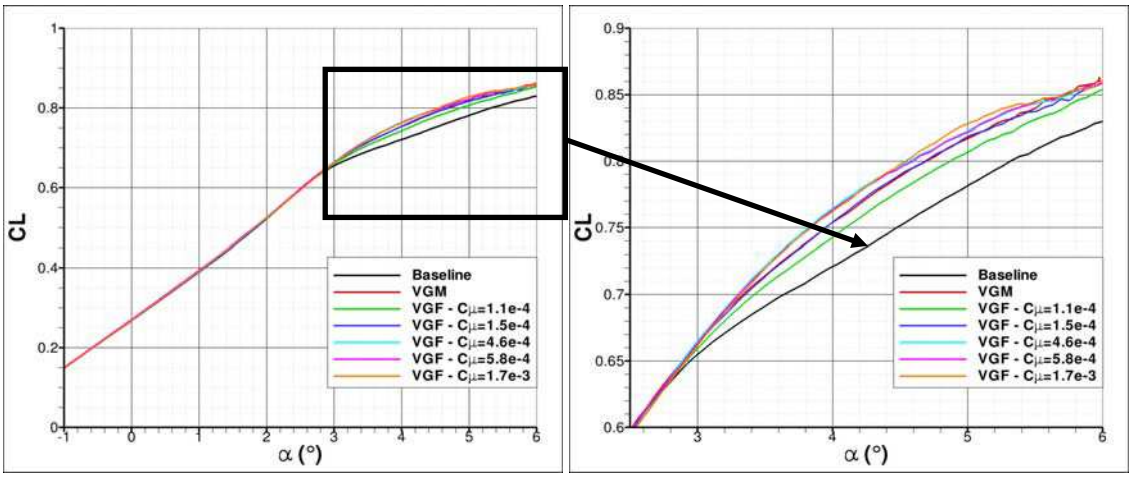


Figure 10 – Lift change with the angle of attack for the baseline, the mechanical VGs and some selected fluidic VGs cases ($M$ = 0.82, $Re_c$=2.83 $10^6$).

## 4.2 Pulsed blowing

The wall pressure distributions for the baseline, the continuous blowing VGs and the pulsed fluidic VGs case at a mass flow rate of 4 g.s$^{-1}$ are given in Figure 11 for an angle-of-attack of 4.25° and $y/b$ = 72.5%. The actuator command varies between 0 and 100% of the fluidic VGs opening. As for the continuous blowing fluidic VGs, the effect of the pulsed fluidic VGs is to suppress the flow separation characterized by the $Cp$ increase at the trailing edge, which occurs for $a \geq 3°$ for the baseline and to shift the shock downstream. The effect of the forcing frequency of the pulsed fluidic VGs is to modify the $Cp$ gradient at the shock foot at around 50% of the chord: for $f$ = 65 and 125 Hz, this gradient is smaller than in the continuous blowing case and than that for pulsed fluidic VGs with $f \geq$ 185 Hz. This lower $Cp$ gradient characterizes in 2D the shock motion on the suction of the airfoil so here, for a forcing frequency of 65 and 125 Hz, the shock motion amplitude is increased compared to the baseline.

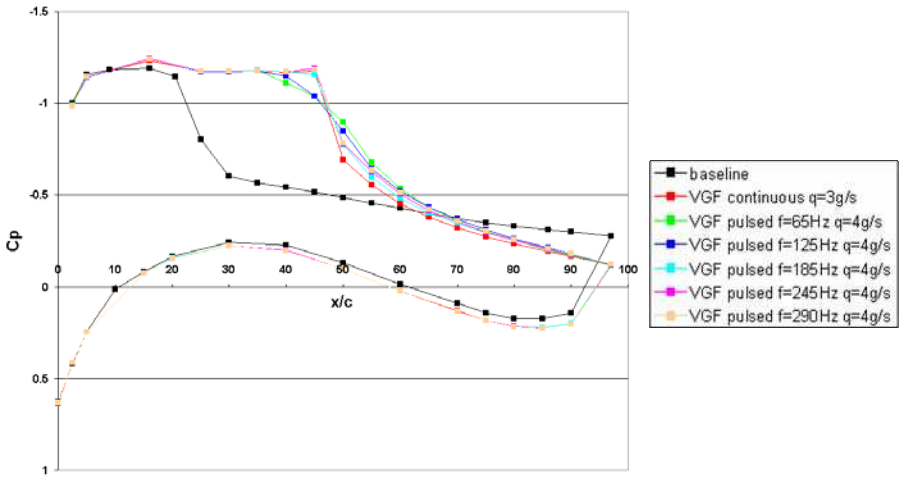


Figure 11 - Wall pressure distribution for the baseline, continuous blowing fluidic VGs and pulsed fluidic VGs at 4.25° and different frequencies at 4 g.s$^{-1}$ and an actuator command between 0 and 100%.

## 5 Buffet control by fluidic TED

The fluidic TED consists in a slot located on the lower side of the model at the trailing-edge. The blowing angle is normal to the lower surface (see Figure 12). Its design is similar to that developed by LEA [3] for the VZLU WT tests during the AVERT European project [6]. The slot is located at $x/c$ = 95% and its width is equal to 0.5 mm. The spanwise length of the slot is 490 mm (between 45% and 85% of wing span). The design of the plenum that supplies the slot with air is

based on the TED design for VZLU tests: 4 transverse sections can be feed separately, the maximum mass flow being equal to 180 g.s$^{-1}$ (4×45 g.s$^{-1}$).

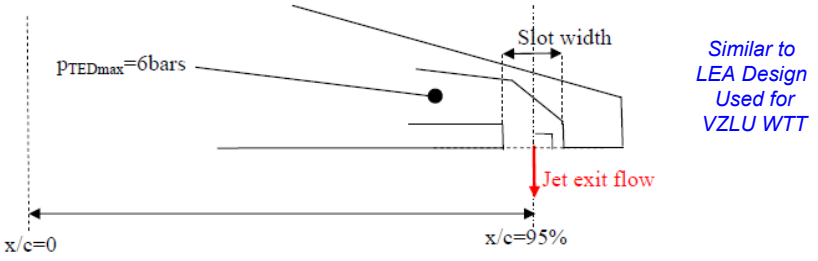


Figure 12 – Sketch showing the definitions of the main parameters of the fluidic TED.

The lift change with the angle-of-attack is given in Figure 13. The effect of the fluidic TED is a constant increase in its value over the entire angle-of-attack range. This global variation on $C_L$ is progressive with the increase of the $C_\mu$. Up to the maximal value of $C_\mu$ (0.0090), corresponding to the maximal mass flow rate of the test device, the observed effects vary linearly with $C_\mu$: the effect for $C_\mu$ = 0.0090 is approximately three times that for $C_\mu$ = 0.0027.

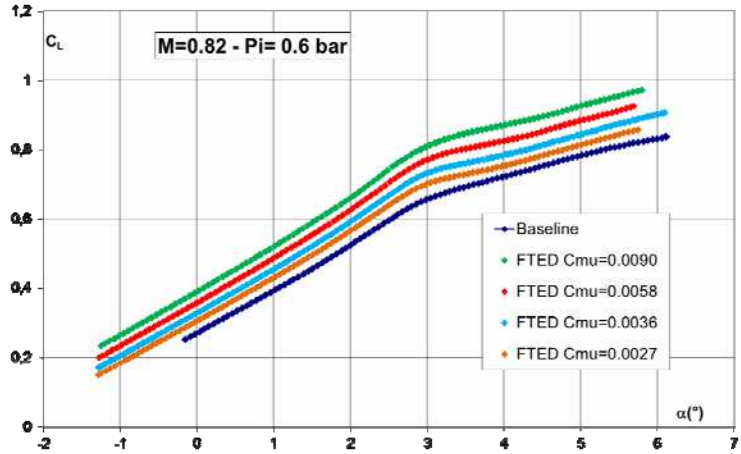


Figure 13 – Fluidic TED action (up to the maximal value of the blowing mass flow rate) on the lift versus $a$ ($M$=0.82, $Re_c$=2.83 10$^6$).

The static wall pressure distributions for the baseline and the fluidic TED are given in Figure 14 for different $C_\mu$ values at the same lift coefficient value. This constant lift coefficient value 0.66 corresponds to the buffet appearance for the baseline configuration ($\alpha$ ~3°). For the fluidic TED cases, the buffet level is lower and close to the buffet onset limit, which can be estimated at $\alpha$ = 2.75°, as well as for baseline than for FTED cases. When the fluidic TED slot is not blowing (slot open - dashed line) there are only slight differences in the pressure distributions compared to the baseline configuration case. For this section at $y/b$ = 72.5%, the strong upper side shock wave moves downstream (10% to 15% of the chord), while the wide supersonic plateau upstream of it becomes lower. On the aft part of the wing, the pressure distribution is "opening", both on the upper and lower side.

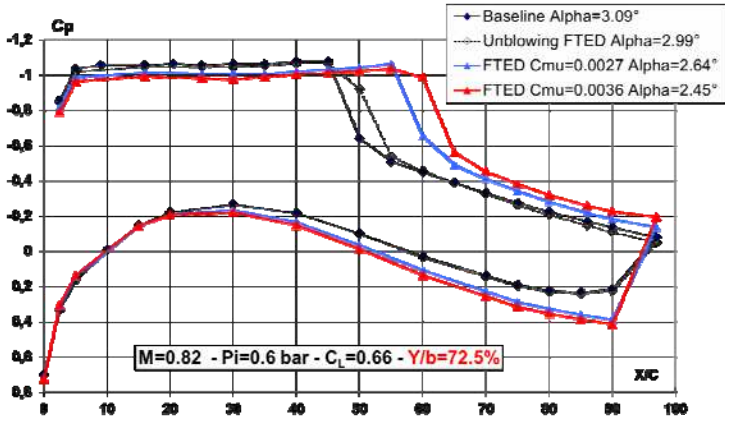


Figure 14 – Wall pressure distributions ($M$=0.82, $Re_c$=2.83 $10^6$): increasing fluidic TED effect at a constant value of the lift coefficient $C_L$=0.66 corresponding to buffet onset.

## 6 Open loop results summary

Figure 15 summarizes the behaviour concerning buffet onset and development for the mechanical and fluidic VG configurations at different $C_\mu$ levels, in comparison with the baseline configuration at $M$ = 0.82 and $Re_c$=2.83 $10^6$. The RMS fluctuations values are plotted versus the angle of attack and versus the lift coefficient for the upper side Kulite pressure transducer named K2, located near the trailing edge at $x/c$ = 85% on the spanwise section $y/b$ = 75%.

At low values of $a$ or lift coefficient, fluidic or mechanical VGs do not produce any increase of the mechanical vibration level. For mechanical VGs, the strong increase in the pressure fluctuation and mechanical vibration corresponding to buffet is clearly postponed to higher angle of attack and lift values. Moreover, the increase in the pressure fluctuation seems to be reduced when buffet becomes stronger. The buffet onset limit is estimated at $a$ = 3° (instead of 2.75° for baseline). For fluidic VGs, the effects are similar, but stronger. At $C_\mu$ = 0.0006, the buffet onset limit can be estimated at $a$ = 3.25° and the increase in the pressure fluctuation when buffet develops is lower, as for the baseline or even the mechanical VGs configuration.

Concerning the control by the fluidic TED, it is important to note that this flow control device does not delay the buffet onset at higher angles of attack (see Figure 15 (left)) but only at higher lift values (see Figure 15 (right)), since, as was shown in Figure 13, the effect is a constant lift increase over the entire angle-of-attack range and the kink visible on the lift curve at around 3° is not delayed by the fluidic TED.

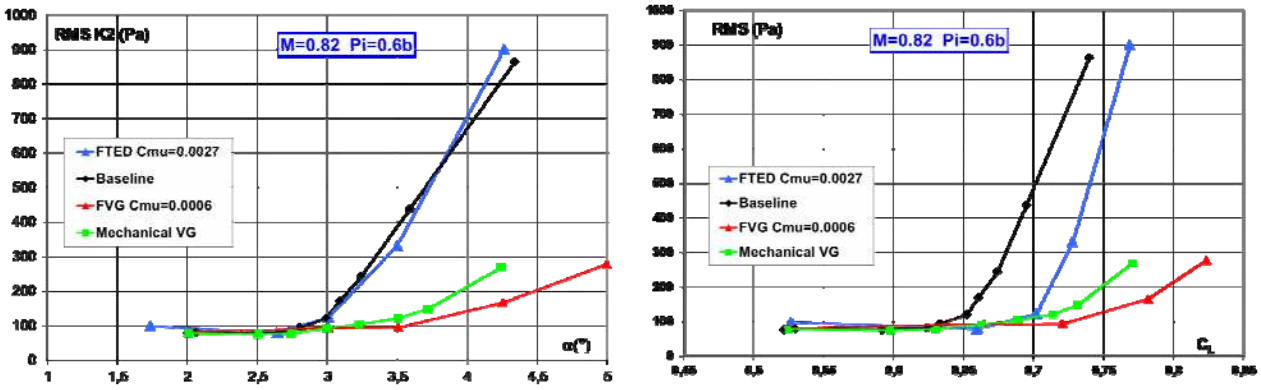


**Figure 15 – Buffet entrance with fluidic and mechanical VGs; comparison with the baseline configuration at M=0.82 and Pi=0.6bar: unsteady wall pressure measurements.**

## 7 Conclusion

The aim of this paper was to summarize the work performed at Onera over the last decade within the framework of several European and self-funded projects. The efficiency of flow control

devices has been evaluated in two wind tunnels under transonic flow conditions, at different Mach and Reynolds numbers. These results, recorded in an industrial-type environment, have allowed the behaviour of such active technologies to be assessed and them to be brought to TRL "Technology Readiness Level" values of 3-4.The effects of both passive and active devices are to:

- postpone buffet onset at a higher angles of attack (mechanical/fluidic VGs), or at higher lift values (all);
- decrease the extent of separated areas (from oil-flow visualizations and mini-tufts);
- decrease the unsteadiness (records provided by Kulite transducers and accelerometers);
- increase the lift coefficient for high angles of attack (from force measurements).

Many parametric investigations were performed (not all shown here) for different fluidic VG spacings, spanwise locations and also mass flow rates, and thus momentum coefficients.

The effect of the fluidic VGs is similar to that of the mechanical VGs, with a saturation reached for momentum coefficient $C_\mu$ above $9\ 10^{-5}$, corresponding to a flow rate of 0.12 $g.s^{-1}$ per hole. Fluidic VGs at $C_\mu$ of $6\ 10^{-5}$ have very similar aerodynamic performances to those of the mechanical VGs case. The effect on unsteady components is very similar.

Concerning the fluidic TED, a linear-type behaviour has been noted on the lift coefficient. It should be pointed out that the efficiency of a fluidic TED with $C_\mu$=0.0027 corresponds to that of a mechanical TED or mini-flap deflected at ~30° when comparing to former results obtained by ONERA.

The closed-loop buffet control using either fluidic VGs or fluidic TED is presented in the companion paper named "Part 2: closed-loop control".

## Acknowledgements

*The AVERT wind tunnel tests were conducted within the FP7 AVERT European project (Contract No.: AST5-CT-2006-030914), funded by EC and project partners (Airbus, Dassault Aviation and Alenia Aeronautica). The closed-loop buffet control tests in the S3Ch wind tunnel, as well as the synthetic jet tests in the S2MA wind tunnel, have received funding from the European Union's Seventh Framework Program (FP7/2007-2013) for the Clean Sky Joint Technology Initiative, under Grant Agreement CSJU-GAM-SFWA-2008-001. The authors are very grateful to the ONERA S3Ch and S2MA wind tunnel teams, who contributed to the success of these tests.*

## References

[1] E. Coustols, V. Brunet, R. Bur, D. Caruana & D. Sipp, 2009, *"BUFET'N Co: A Joint ONERA Research Project devoted to Buffet Control on a Transonic 3D Wing using a Closed-Loop Approach"*, CEAS/KATNET II Conference, Bremen, Germany.

[2] J. Dandois, P. Molton, A. Lepage, A. Geeraert, V. Brunet, J.-B. Dor and E. Coustols, 2013, *Buffet Characterisation and Control for Turbulent Wings*, Aerospace Lab, vol. 6.

[3] G. Browaeys, H. Deniau, E. Collin and J.-P. Bonnet, 2008, *Pneumatic control strategies for transonic buffet. A numerical approach*, 7th International Symposium on Engineering Turbulence Modeling and Measurement (ETMM7), Limassol.

[4] P. Molton, J. Dandois, A. Lepage, V. Brunet & R. Bur, 2013, "*Control of Buffet Phenomenon on a Transonic Swept Wing*", AIAA Journal, Vol. 51, No. 4, pp.761-772.

[5] J. Dandois, V. Brunet, P. Molton, J.-C. Abart & A. Lepage, 2010, *Buffet Control by Means of Mechanical and Fluidic Vortex Generators*, AIAA Paper 2010-4975, 5th AIAA Flow Control Conference, Chicago.

[6] J. Dandois, C. Gleyzes, J.-B. Dor, F. Ternoy & E. Coustols, 2010, *Report on the VZLU wind tunnel test analysis & report on the 3D RANS and URANS computations of mechanical/fluidic VGs and fluidic TEDs*, AVERT deliverables D1.3-3 & D1.3-8.